

NEUTRON STAR EQUATION OF STATE FROM THE QUARK LEVEL IN THE LIGHT OF GW170817

ZHEN-YU ZHU¹, EN-PING ZHOU², ANG LI¹

¹Department of Astronomy, Xiamen University, Xiamen, Fujian 361005, China; liang@xmu.edu.cn

²State Key Laboratory of Nuclear Science and Technology and School of Physics, Peking University, Beijing 100871, China

ABSTRACT

Matter state inside neutron stars is an exciting problem in astrophysics, nuclear physics and particle physics. The equation of state (EOS) of neutron stars plays a crucial role in the present multimessenger astronomy, especially after the event of GW170817. We propose a new neutron star EOS “QMF18” from the quark level, which describes well robust observational constraints from free-space nucleon, nuclear matter saturation, heavy pulsar measurements and the tidal deformability of the very recent GW170817 observation. For this purpose, we employ the quark-mean-field (QMF) model, allowing one to tune the density dependence of the symmetry energy and study effectively its correlations with the Love number and the tidal deformability. We provide tabulated data for the new EOS and compare it with other recent EOSs from various many-body frameworks.

Keywords: dense matter - equation of state - stars: neutron - gravitational waves

1. INTRODUCTION

Neutron stars (NSs) are by far one of the most interesting observational objects, since many mysteries remain on them due to their complexity. Multimessenger observations with advanced telescopes such as Advanced LIGO and VIRGO (e.g., [Abbott et al. 2017](#)), FAST (e.g., [Li & Pan 2016](#)), SKA (e.g., [Watts et al. 2015](#)), NICER (e.g., [Özel et al. 2016](#)), HXMT (e.g., [Li et al. 2018b](#)), eXTP (e.g., [Watts et al. 2018](#)), AXTAR (e.g., [Ray et al. 2010](#)), will hopefully provide precise measurements of their mass and/or radius, thus improving our current knowledge of such stellar objects and their equation of states (EOSs), especially for the high-density inner crust with densities above nuclear saturation density $\rho_0 \sim 0.16 \text{ fm}^{-3}$. Dense matter EOS is also closely related to the scientific goals of all advanced radioactive beam facilities being built around the world (e.g., [Danielewicz et al. 2002](#); [Tsang et al. 2009](#)).

Nowadays, the EOS of symmetric nuclear matter (SNM) ([Danielewicz et al. 2002](#)) ($\beta \equiv \frac{\rho_n - \rho_p}{\rho_n + \rho_p} = 0$) is relatively well-constrained, with ρ_n, ρ_p , the neutron, proton density, respectively. Matter with nonzero isospin asymmetry remains unknown, largely due to the uncertainty in the symmetry energy: $E_{\text{sym}}(\rho) \approx [E(\rho, \beta) - E(\rho, 0)]/\beta^2$, with $E(\rho, \beta)$ the energy per nucleon of nuclear matter at isospin asymmetry β and density ρ . Conflicts remains for the symmetry energy (especially its slope $L(\rho) = dE_{\text{sym}}(\rho)/d\rho$) despite significant progress in constraining the symmetry energy around and below nuclear matter saturation density (e.g., [Tsang et al. 2009](#); [Danielewicz & Lee 2014](#); [Zhang & Chen 2015](#)). At saturation density $\rho = \rho_0$, L may has a lower limit $\sim 20 \text{ MeV}$ ([Centelles et al. 2009](#)) and an upper limit $> 170 \text{ MeV}$ ([Cozma et al. 2013](#)). It characterizes the density dependence of the symmetry energy and largely dominates the ambiguity and stiffness of EOS for dense nuclear matter and NS matter at densities approached in NS cores, in the case of no strangeness phase transition (e.g., [Burgio et al. 2011](#); [Hu et al. 2014b](#); [Li et al. 2006, 2007, 2010, 2015](#); [Zhu et al. 2016](#)). Therefore it is a crucial parameter for NS EOS and related studies.

Recently from the observation of GW170817, the LIGO+Virgo Collaborations placed a clean upper limit on the tidal deformability of the compact object, $\Lambda = (2/3)k_2/(GM/c^2R)^5$ with k_2 is the second Love number. Since the star radius is rather sensitive to the symmetry energy (essentially its slope L) with the maximum mass only slightly modified (e.g., [Lattimer & Prakash 2004, 2001](#); [Li & Steiner 2006](#)), possibly this Λ measurement might put independent constraint on L , as has been previously discussed in [Fattoyev et al. \(2013, 2018\)](#); [Zhang et al. \(2018\)](#). Λ describes the amount of induced mass quadrupole moment when reacting to a certain external tidal field ([Damour et al. 1992](#); [Damour & Nagar 2009](#)). If a low spin prior is assumed for both stars in the binary, which is reasonable considering the magnetic braking during the binary evolution, the tidal deformability for a $1.4 M_\odot$ star (denoted as $\Lambda(1.4)$ in below) was concluded to be smaller than 800 (a more loosely constrained upper limit of 1400 is found for the high-spin prior case) ([Abbott et al. 2017](#)). Based on the GW170817 observation, several recent studies have reported their constrains

on NS EOS (e.g., Ai et al. 2018; Annala et al. 2018, 2017; Bauswein et al. 2017; Drago & Pagliara 2018; Fattoyev et al. 2018; Krastev & Li 2018; Ma et al. 2017; Margalit & Metzger 2017; Nandi & Char 2018; Paschalidis et al. 2018; Radice et al. 2018; Ruiz et al. 2018; Shibata et al. 2017; Zhang et al. 2018) and QS EOS (Zhou et al. 2018).

The objective of the present study is to make use of the new GW170817 constraint, combined with available terrestrial nuclear structure/reaction experiments (e.g., Danielewicz et al. 2002; Tsang et al. 2009; Li & Han 2013; Danielewicz & Lee 2014; Zhang & Chen 2015) and astrophysical observations (Antoniadis et al. 2013; Demorest et al. 2010; Fonseca et al. 2016) for the determination of nuclear saturation properties, and to construct a new NS EOS from the quark level. The employed EOS model enables us to fine tune the L value and study consistently the Λ vs L dependence, with well-reproduced robust observables from laboratory nucleons, nuclear saturation, heavy-ion collisions (HIC) and heavy pulsars.

The paper is organized as follows. In Section 2, we describe the theoretical framework to describe consistently a nucleon and many-body nucleonic system from a quark potential, including the necessary fitting of the quark potential parameters and the meson coupling parameters from vacuum nucleon and empirical nuclear saturation properties, respectively. In Section 3, the NS EOSs and the corresponding mass-radius relations as well as the tidal deformabilities are discussed, to be compared with the mass measurements of heavy pulsars (Antoniadis et al. 2013; Demorest et al. 2010; Fonseca et al. 2016) and the tidal deformability of GW170817 (either $\Lambda(1.4)$ or $\tilde{\Lambda}$) (Abbott et al. 2017); Tabulated EOS of the new ‘‘QMF18’’ model is also provided and comparisons are made with other recent EOSs from various many-body theories. Summary and future perspective finally presented in Section 4.

2. MODEL

To carry out a study of nuclear many-body system from the quark level, one first constructs a nucleon from confined quarks, by a finite confining region (characterized by a constant energy per unit volume, the bag constant B) (Chodos et al. 1974) or by constituent quarks with a harmonic oscillator confining potential (Barik & Dash 1986; Frederico et al. 1989). Then nucleons interact with point-like mesons. Since the meson fields modify the internal quark motion, the mesons couple not to point-like nucleons but self-consistently to confined quarks. The effect of the nucleon velocity as well as the effect of antisymmetrisation are usually neglected, and the calculation is done in the mean-field approximation. The first model is often called the quark-meson coupling (QMC) (e.g., Barik et al. 2013; Guichon 1988; Mishra et al. 2015, 2016; Saito et al. 2007), and the later is called the quark mean-field (QMF) model (e.g., Hu et al. 2014a,b; Shen & Toki 2000, 2002; Toki et al. 1998; Xing et al. 2016; Zhu & Li 2018). The QMC and QMF models may be viewed as variation of the relativistic mean-field (RMF) model (e.g., Boguta & Bodmer 1977; Horowitz & Piekarewicz 2001; Müller & Serot 1996; Serot & Walecka 1986; Walecka 1974) which is from the hadron level. The RMF model, including its extension of the isoscalar Fock terms (e.g., Li et al. 2018a; Long et al. 2012; Sun et al. 2008; Zhu et al. 2016), has been widely-used for NS studies.

In this work, following the methodology of the QMC and QMF models, we start with a flavor independent potential $U(r)$ confining the constituent quarks inside a nucleon. Details can be found in Barik et al. (2013); Mishra et al. (2015, 2016); Xing et al. (2016); Zhu & Li (2018). Here for completeness, we only write necessary formulas. The confining potential is written as (Barik & Dash 1986):

$$U(r) = \frac{1}{2}(1 + \gamma^0)(ar^2 + V_0), \quad (1)$$

with the parameters a and V_0 to be determined from vacuum nucleon properties. The Dirac equation of the confined quarks is written as

$$[\gamma^0(\epsilon_q - g_{\omega q}\omega - \tau_{3q}g_{\rho q}\rho) - \vec{\gamma} \cdot \vec{p} - (m_q - g_{\sigma q}\sigma) - U(r)]\psi_q(\vec{r}) = 0, \quad (2)$$

Hereafter $\psi_q(\vec{r})$ is the quark field, σ , ω , and ρ are the classical meson fields. $g_{\sigma q}$, $g_{\omega q}$, and $g_{\rho q}$ are the coupling constants of σ , ω , and ρ mesons with quarks, respectively. τ_{3q} is the third component of isospin matrix. This equation can be solved exactly and its ground state solution for energy is

$$(\epsilon'_q - m'_q)\sqrt{\frac{\lambda_q}{a}} = 3, \quad (3)$$

where $\lambda_q = \epsilon_q^* + m_q^*$, $\epsilon'_q = \epsilon_q^* - V_0/2$, $m'_q = m_q^* + V_0/2$. The effective single quark energy is given by $\epsilon_q^* = \epsilon_q - g_{q\omega}\omega - \tau_{3q}g_{q\rho}\rho$ and the effective quark mass by $m_q^* = m_q - g_{\sigma q}\sigma$ with the quark mass $m_q = 300$ MeV.

The zeroth-order energy of the nucleon core $E_N^0 = \sum_q \epsilon_q^*$ can be obtained by solving Eq. (3). The contribution of center-of-mass correction $\epsilon_{c.m.}$, pionic correction δM_N^π and gluonic correction $(\Delta E_N)_g$ are also taken into account as

Table 1. Saturation properties used in this study for the fitting of new sets of meson coupling parameters: The saturation density ρ_0 (in fm^{-3}) and the corresponding values at saturation point for the binding energy E/A (in MeV), the incompressibility K (in MeV), the symmetry energy E_{sym} (in MeV), the symmetry energy slope L (in MeV) and the ratio between the effective mass and free nucleon mass M_N^*/M_N .

ρ_0 [fm^{-3}]	E/A [MeV]	K [MeV]	E_{sym} [MeV]	L [MeV]	M_N^*/M_N /
0.16	-16	240	31	20/40/60/80	0.77

Table 2. Newly fitted meson coupling parameters by using Table 1 as input.

L [MeV]	$g_{\sigma q}$	$g_{\omega q}$	$g_{\rho q}$	g_2 [fm^{-1}]	g_3	Λ_v
20	3.8620366	2.9174838	6.9588083	14.6179599	-66.3442468	1.1080665
40	3.8620366	2.9174838	5.4129448	14.6179599	-66.3442468	0.7693664
60	3.8620366	2.9174838	4.5830609	14.6179599	-66.3442468	0.4306662
80	3.8620366	2.9174838	4.0459574	14.6179599	-66.3442468	0.0919661

done in Barik et al. (2013); Barik & Dash (1986); Mishra et al. (2015, 2016); Xing et al. (2016); Zhu & Li (2018). With these corrections on energy, we can then determine the mass of nucleon in medium:

$$M_N^* = E_N^0 - \epsilon_{c.m.} + \delta M_N^\pi + (\Delta E_N)_g. \quad (4)$$

The nucleon radius is written as

$$\langle r_N^2 \rangle = \frac{11\epsilon'_q + m'_q}{(3\epsilon'_q + m'_q)(\epsilon_q^2 - m_q^2)}. \quad (5)$$

From reproducing the nucleon mass and radius (M_N, r_N) in free space, we determine the potential parameters (a and V_0) in Eq. (1). $V_0 = -62.257187$ MeV and $a = 0.534296$ fm^{-3} are obtained by fitting $M_N = 939$ MeV and $r_N = 0.87$ fm.

We then move from a single nucleon to nucleonic many-body system for the study of infinite nuclear matter and NSs. Nuclear matter is described by point-like nucleons and mesons interacting through exchange of σ , ω , ρ mesons. The Lagrangian is written as (see also for example in Li et al. (2008)):

$$\begin{aligned} \mathcal{L} = & \bar{\psi} (i\gamma_\mu \partial^\mu - M_N^* - g_{\omega N} \omega \gamma^0 - g_{\rho N} \rho \tau_3 \gamma^0) \psi - \frac{1}{2} (\nabla \sigma)^2 - \frac{1}{2} m_\sigma^2 \sigma^2 - \frac{1}{3} g_2 \sigma^3 - \frac{1}{4} g_3 \sigma^4 \\ & + \frac{1}{2} (\nabla \rho)^2 + \frac{1}{2} m_\rho^2 \rho^2 + \frac{1}{2} (\nabla \omega)^2 + \frac{1}{2} m_\omega^2 \omega^2 + \frac{1}{2} g_{\rho N}^2 \rho^2 \Lambda_v g_{\omega N}^2 \omega^2, \end{aligned} \quad (6)$$

where $g_{\omega N}$ and $g_{\rho N}$ are the nucleon coupling constants for ω and ρ mesons. From the quark counting rule, we obtain $g_{\omega N} = 3g_{\omega q}$ and $g_{\rho N} = g_{\rho q}$. The calculation of confined quarks gives the relation of effective nucleon mass M_N^* as a function of σ field, which defines the σ coupling with nucleons (depending on the parameter $g_{\sigma q}$). $m_\sigma = 510$ MeV, $m_\omega = 783$ MeV, and $m_\rho = 770$ MeV are the meson masses.

The equations of motion for mesons can be obtained by variation of the Lagrangian:

$$(i\gamma^\mu \partial_\mu - M_N^* - g_{\omega N} \omega \gamma^0 - g_{\rho N} \rho \tau_3 \gamma^0) \psi = 0, \quad (7)$$

$$m_\sigma^2 \sigma + g_2 \sigma^2 + g_3 \sigma^3 = -\frac{\partial M_N^*}{\partial \sigma} \langle \bar{\psi} \psi \rangle, \quad (8)$$

$$m_\omega^2 \omega + \Lambda_v g_{\omega N}^2 g_{\rho N}^2 \omega \rho^2 = g_{\omega N} \langle \bar{\psi} \gamma^0 \psi \rangle, \quad (9)$$

$$m_\rho^2 \rho + \Lambda_v g_{\rho N}^2 g_{\omega N}^2 \rho \omega^2 = g_{\rho N} \langle \bar{\psi} \tau_3 \gamma^0 \psi \rangle. \quad (10)$$

From these Lagrangian and equations of motion of nucleon and mesons, the energy density and pressure can be generated by the energy-momentum tensor:

$$\begin{aligned} \mathcal{E} = & \frac{1}{\pi^2} \sum_{i=n,p} \int_0^{k_F^i} \sqrt{k^2 + M_N^{*2}} k^2 dk + \frac{1}{2} m_\sigma^2 \sigma^2 + \frac{1}{3} g_2 \sigma^3 + \frac{1}{4} g_3 \sigma^4 \\ & + \frac{1}{2} m_\omega^2 \omega^2 + \frac{1}{2} m_\rho^2 \rho^2 + \frac{3}{2} \Lambda_v g_{\rho N}^2 g_{\omega N}^2 \rho^2 \omega^2, \end{aligned} \quad (11)$$

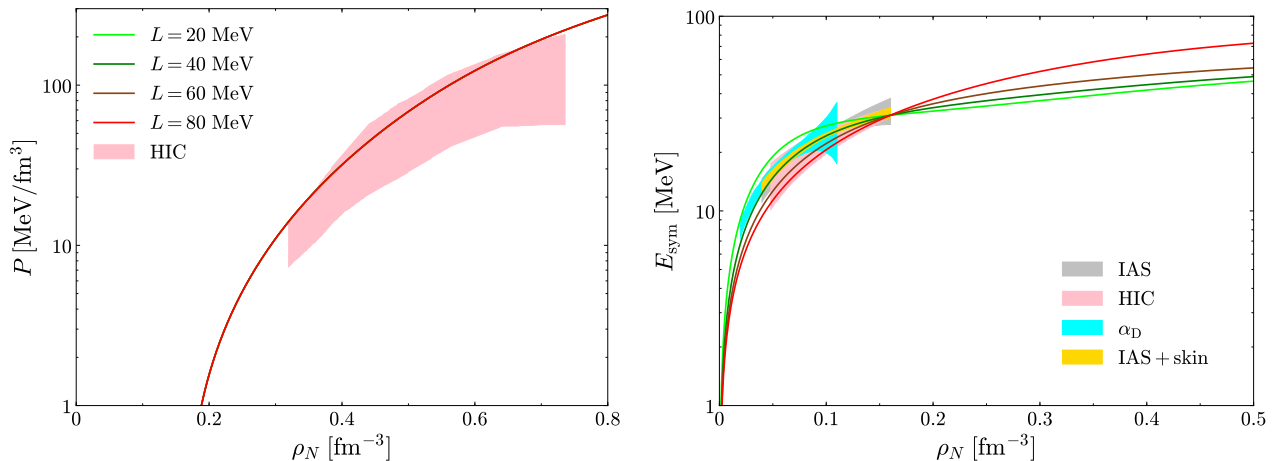


Figure 1. (Left panel) Pressure as a function of nucleon number density for SNM, together with the constraint from collective flow in HIC (Danielewicz et al. 2002) (Note here that the results from different parameter sets with different value of symmetry energy slope L are the same in SNM); (Right panel) Symmetry energy as a function of nucleon number density with four different values of symmetry energy slope L . Colorful shadow regions represent the constraints from isobaric analog states (IAS) and from transport in HIC (Tsang et al. 2009), electric dipole polarizability in ^{208}Pb (α_D) (Zhang & Chen 2015), IAS and neutron skins (IAS+skin) (Danielewicz & Lee 2014), respectively.

$$\begin{aligned}
 P = & \frac{1}{3\pi^2} \sum_{i=n,p} \int_0^{k_F^i} \frac{k^4}{\sqrt{k^2 + M_N^{*2}}} dk - \frac{1}{2} m_\sigma^2 \sigma^2 - \frac{1}{3} g_2 \sigma^3 - \frac{1}{4} g_3 \sigma^4 \\
 & + \frac{1}{2} m_\omega^2 \omega^2 + \frac{1}{2} m_\rho^2 \rho^2 + \frac{1}{2} \Lambda_v g_{\rho N}^2 g_{\omega N}^2 \rho^2 \omega^2.
 \end{aligned} \tag{12}$$

k_F^p (k_F^n) is the Fermi momentum for proton (neutron).

There are six parameters ($g_{\sigma q}, g_{\omega q}, g_{\rho q}, g_2, g_3, \Lambda_v$) in the Lagrangian of Eq. (6) and they will be determined by fitting the saturation density ρ_0 and the corresponding values at saturation point for the binding energy E/A , the incompressibility K , the symmetry energy E_{sym} , the symmetry energy slope L and the effective mass M_N^* . Those employed values are collected in Table 1. We use the intermediate value of incompressibility $K \approx 240 \pm 20$ MeV from Piekarewicz (2010); Shlomo et al. (2006). We also employ the most preferred values for (E_{sym}, L) newly suggested by Li & Han (2013), namely $E_{\text{sym}} = 31.6 \pm 2.66$ MeV, $L \approx 58.9 \pm 16$ MeV. Since the L value can be as low as ~ 20 MeV (Centelles et al. 2009), we choose four values of L (20, 40, 60, 80 MeV) as input of the parameter fitting according to our model capability, for studying its effect on the tidal deformability of binary NS system (Abbott et al. 2017). The modal parameters obtained are collected in Table 2. Note that in our previous work (Zhu & Li 2018), with similar proper saturation properties ($\rho_0, E/A, K, E_{\text{sym}}, L, M_N^*$) from terrestrial dense-matter measurements, the high-density EOS failed to reproduce the two-solar-mass-constraint from massive pulsars (only around 1.6 times the solar mass). For the present purpose of introducing new EOS for astrophysical studies, we refit the parameters by omitting the nonlinear terms of ω meson field and successfully obtain a maximum mass fulfilling the two-solar-mass constraint for the first time within QMF.

3. EOS, MASS-RADIUS RELATION AND TIDAL DEFORMABILITY

After the meson coupling parameters are established, the pressure and symmetry energy as functions of density for nuclear matter can be calculated. The results are shown in Figure 1, together with experimental regions (Danielewicz et al. 2002; Danielewicz & Lee 2014; Tsang et al. 2009; Zhang & Chen 2015). In the left panel, one can see that the SNM EOS is compatible with the flow constraint (Danielewicz et al. 2002). In the right panel for different L , the behaviour of symmetry energy vs density are all consistent with various nuclear experiments. Among them, the $L = 40$ MeV case lies comfortably inside all experimental boundaries.

We can move forward to calculate the EOS of NS matter, $P(\mathcal{E})$, by introducing β -equilibrium and charge neutrality condition between nucleons and leptons:

$$\mu_n = \mu_e + \mu_p, \quad \rho_e + \rho_\mu = \mu_p, \tag{13}$$

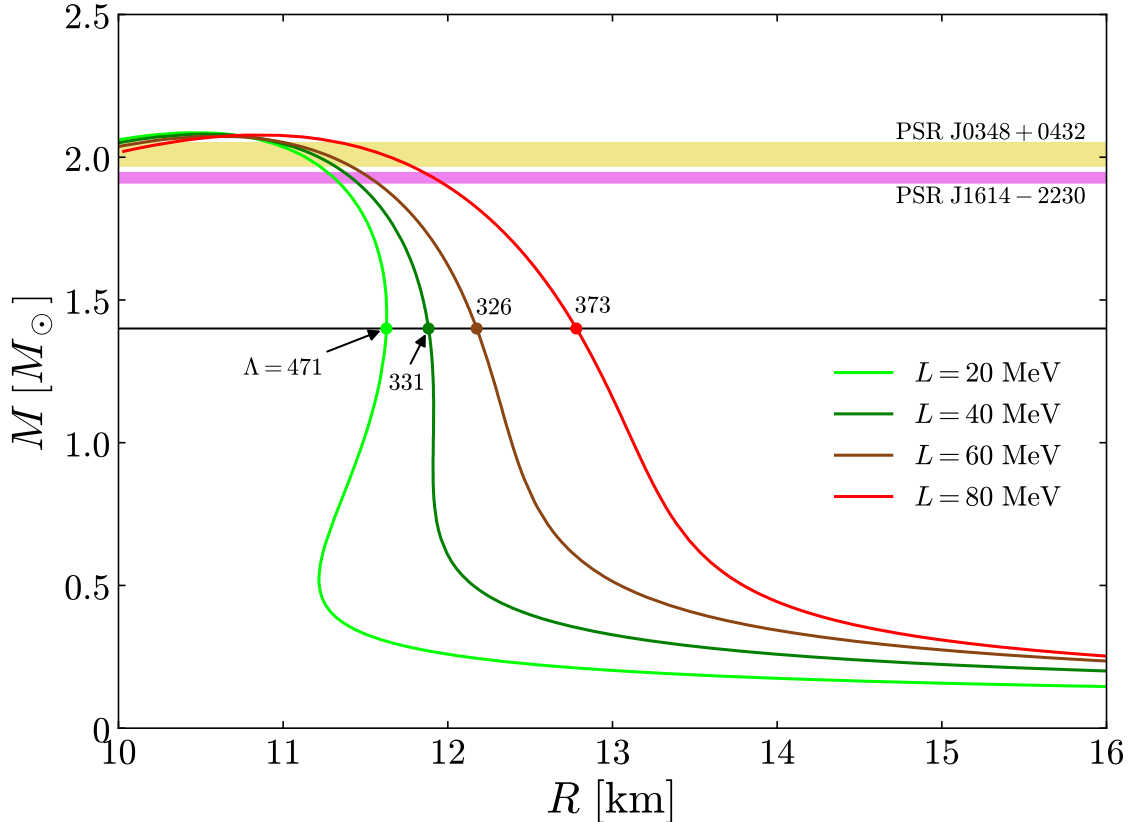


Figure 2. Mass-radius curves for four EOSs with different value of L (20, 40, 60, 80 MeV), together with the mass measurements for two recent massive stars: PSR J1614-2230 (Demorest et al. 2010; Fonseca et al. 2016) and PSR J0348+0432 (Antoniadis et al. 2013). The horizontal black line indicates $M = 1.4 M_{\odot}$. Numbers mark the Λ values for $1.4 M_{\odot}$ stars corresponding to colourful dots.

where $(\mu_n, \mu_e, \mu_p)/(\rho_n, \rho_e, \rho_p)$ are the chemical potential/number density of neutron, electron and proton, respectively. To describe the structure of the crust, we employ the quantal calculations of Negele & Vautherin (1973) for the medium-density regime ($0.001 \text{ fm}^{-3} < \rho_N < 0.08 \text{ fm}^{-3}$), and follow the formalism developed in Baym et al. (1971) for the outer crust ($\rho_N < 0.001 \text{ fm}^{-3}$). The tidal Love numbers k_2 is obtained from the ratio of the induced quadrupole moment Q_{ij} to the applied tidal field E_{ij} (Damour & Nagar 2009; Damour et al. 1992; Hinderer 2008): $Q_{ij} = -k_2 \frac{2R^5}{3G} E_{ij}$, where R is the NS radius. The dimensionless tidal deformability Λ is related to the compactness M/R and the Love number k_2 through $\Lambda = \frac{2}{3} k_2 (M/R)^{-5}$.

The resulting mass-radius relations with $L = 20, 40, 60, 80$ MeV are presented in Figure 2. They all fulfill the recent observational constraints of the two massive pulsars of which the masses are precisely measured (Antoniadis et al. 2013; Demorest et al. 2010; Fonseca et al. 2016). Since these four EOSs have the same incompressibility ($K = 240$ MeV) and symmetry energy ($E_{\text{sym}} = 31$ MeV) but rather different symmetry energy slope L , it is clearly demonstrated that the radius sensitively depends on the symmetry energy slope with the maximum mass only slightly modified. It is the well accepted R vs L dependence mentioned in the introduction (e.g., Lattimer & Prakash 2004, 2001; Li & Steiner 2006). A smaller L (softer symmetry energy) leads to a smaller radius. The combined results for $\Lambda(1.4)$ are as shown in Figure 2. They all fulfill the GW170817 constraint of $\Lambda(1.4) \leq 800$ (Abbott et al. 2017). Different crust prescriptions could have influence on the resulting radius, we also test the crust dependence of tidal deformability by connecting the $L = 40$ MeV EOS model with four other crust models collected in our previous work (Li et al. 2016b). The resulting $\Lambda(1.4)$ is in the range of $324 \sim 344$, namely in the present study the crust influence of tidal deformability is limited around 6 % for a $1.4 M_{\odot}$ star.

We proceed to present in Figure 3 (Figure 4) the resulting Love numbers (tidal deformabilities) as a function of the mass and the compactness. The behaviours of k_2 and Λ follow the above analysis and are similar with previous calculations (e.g., Hinderer et al. 2010; Postnikov et al. 2010). In Figure 3, k_2 first increases then decreases with the mass and the compactness. In Figure 4, Λ monotonously decreases with the mass and the compactness. The increase

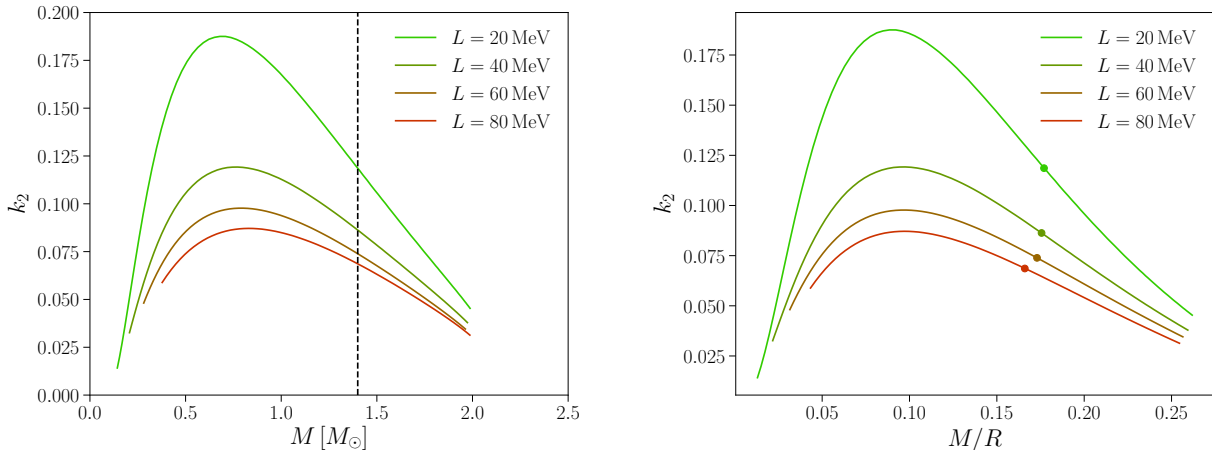


Figure 3. Love numbers as a function of the mass (left panel) and the compactness (right panel), for four EOSs with different value of L (20, 40, 60, 80 MeV). The vertical line and colorful dots indicate $M = 1.4 M_\odot$.

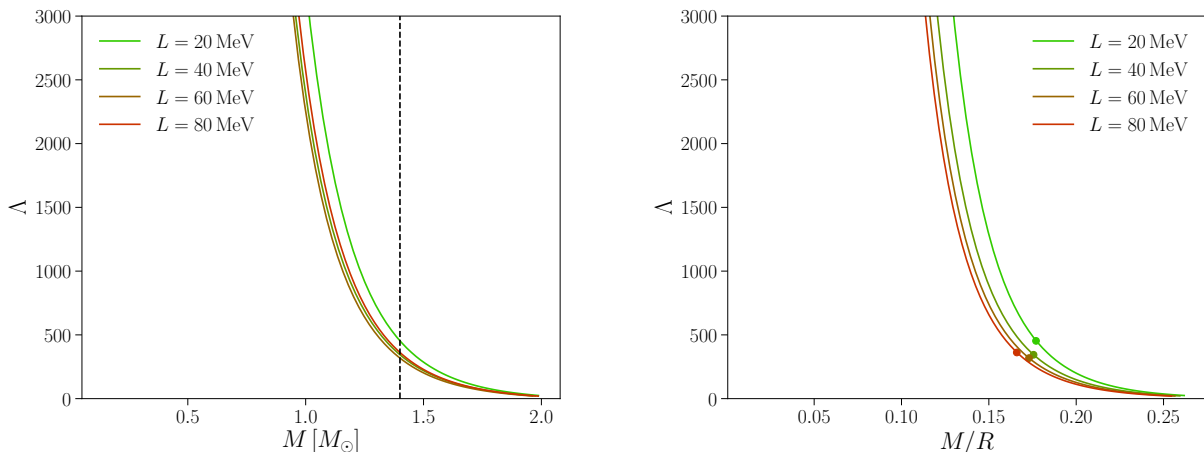


Figure 4. Same with Figure 3, but for the tidal deformabilities.

of k_2 and large values of Λ for small masses (below $\sim 1.0 M_\odot$) are due to large radii and large portion of soft crust matter. If no crust is considered (e.g. an EOS described by a pure polytropic function), k_2 will decrease monotonously with mass and compactness as well (Hinderer et al. 2010).

It's worthy noting that according to Figure 3, k_2 monotonically depends on L for all the mass range, i.e., for a star with certain amount of mass (compactness), a larger L leads to a smaller k_2 . However, as already seen in Figure 2 from $\Lambda(1.4)$, this monotonic dependence doesn't hold for Λ , since Λ is normalized with a factor of R^5 . Hence the differences in radius (according to the R vs L relation mentioned before) will scatter the dependence of Λ on L .

To understand better the relation between L and Λ , we present in Figure 5, for more L values, the results of both $\Lambda(1.4)$ and the measured mass-weighted tidal deformability ($\tilde{\Lambda}$). A chirp mass of $1.188 M_\odot$ and mass ratio of 0.7^1 are employed for the calculation of $\tilde{\Lambda}$ in a binary system. We can see that neither $\Lambda(1.4)$ nor $\tilde{\Lambda}$ shows correlation with L . In general, one expects large Λ at large L since a large star (i.e., large R) tends to be easily deformed. However, Λ is anomalously large at small L (i.e. $L \leq 30$ MeV), which may be understood from the different smoothness behaviour in these cases at the crust-core matching interface, when core EOSs with different L are matched to the same inner crust EOS of Negele & Vautherin (1973). The importance of matching interface has been pointed out also in our previous work (Li et al. 2016b) for the mass-equatorial radius relations of fast spinning NSs and deserve a better study in the future. The violation of monotonic dependence of Λ on L is particularly interesting in terms of observations. As a

¹ As pointed out by (e.g., Radice et al. 2018), the mass-weighted tidal deformability is expected to be very weakly dependent on the mass ratio. Hence considering one mass ratio case should be representative enough for analysis.

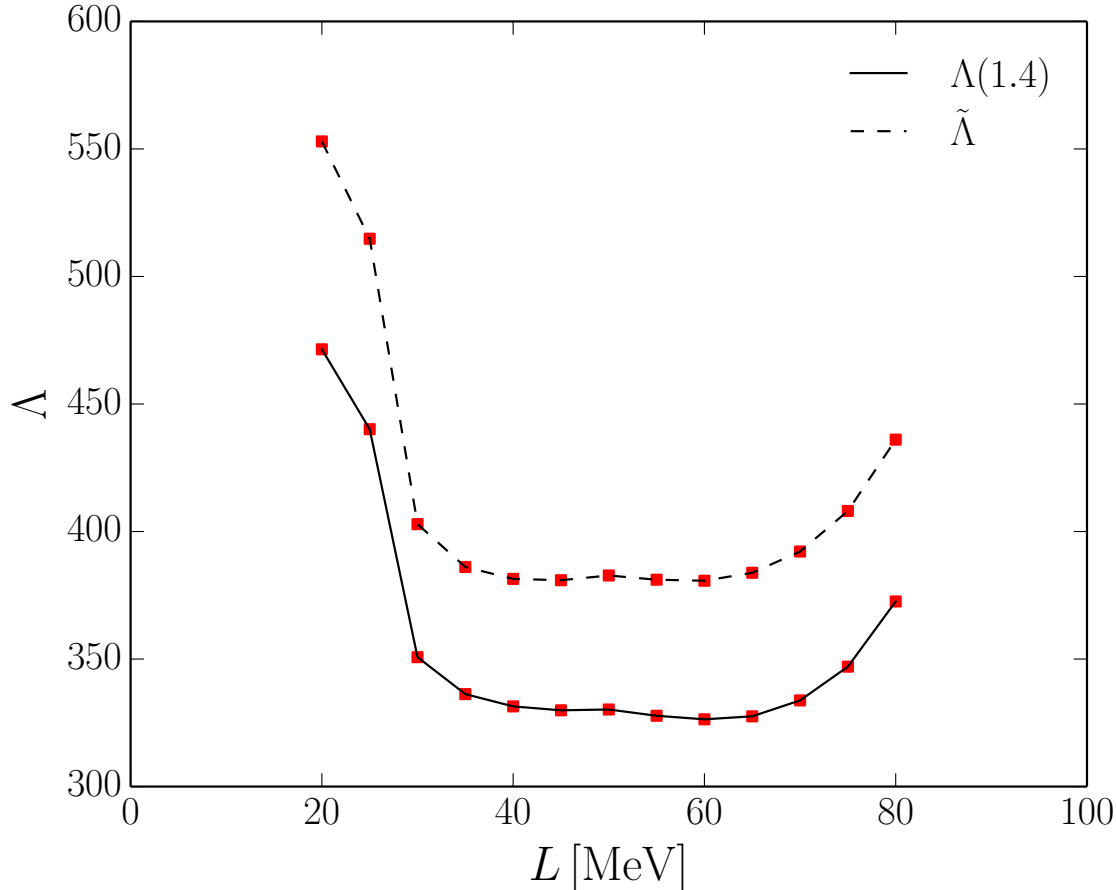


Figure 5. L dependence of tidal deformability: (In solid) the tidal deformability for a $1.4 M_{\odot}$ star and (in dashed) the mass-weighted tidal deformability $\tilde{\Lambda}$ of a binary system with a chirp mass of $1.188 M_{\odot}$, and mass ratio of 0.7 (Abbott et al. 2017).

consequence, a measurement of $\tilde{\Lambda}$ by GW observations doesn't necessarily translate into measurement of radius of the NS, given the R vs L relation. Similar conclusion has been recognized also in the extended Skyrme-Hartree-Fock model (Chen et al. 2018).

Finally in this section, we provide the tabulated EOS in Table 3 for our presently best model (the case of $L = 40$ MeV), with satisfying descriptions of vacuum nucleon properties (r_N, m_N), nuclear matter properties ($\rho_0, E/A, K, E_{\text{sym}}, L, M_N^*$), and astrophysical observations ($M_{\text{TOV}}, \Lambda(1.4)$). It is named as ‘‘QMF18’’ EOS. Without interpolation, the EOS data in Table 3 give $2.0805 M_{\odot}$ for M_{TOV} , within an error of magnitude of $\sim 10^{-4}$: the complete data give $2.0809 M_{\odot}$.

We also collect other new NS EOSs from various many-body techniques. These EOSs with their mass-radius relations are plotted in Figure 6. Their L and M_{TOV} values are also shown in Table 4, with $\tilde{\Lambda}$ and various results for a $1.4 M_{\odot}$ star: $R(1.4)$, $M/R(1.4)$ and $\Lambda(1.4)$. The EOSs of NL3 $\omega\rho$, DDME2, and DD2 are from the RMF model (Fortin et al. 2016). The EOSs of DDRHF and DDRHF Δ is from the density-dependent relativistic Hartree-Fock (DDRHF) theory, with the later one extended to include Δ -isobars (Zhu et al. 2016). The Sly9 EOS is from the Skyrme functional (Fortin et al. 2016). The BCPM EOS, named after Barcelona-Catania-Paris-Madrid energy density functional (Sharma et al. 2015), is based on the microscopic Brueckner-Hartree-Fock theory (Baldo 1999).

We see that the tidal deformability has a roughly positive relation with the symmetry energy slope L : A smaller L usually leads to a smaller $\Lambda(1.4)$. Nevertheless, $\Lambda(1.4)$ depends not only on the saturation properties (like L), but also on the high-density part of EOS (imprinted on M_{TOV}). This is clearly seen in the comparison of the NL3 $\omega\rho$ and DD2 cases, where with the same $L \sim 55$ MeV, $\Lambda(1.4)$ drops from 925 for NL3 $\omega\rho$ to 674 for DD2, resulting from a much lowered M_{TOV} value in the DD2 case: 2.75 vs 2.42 M_{\odot} . We notice that, besides NL3 $\omega\rho$, the DDRHF results with a representative parameter set PKO3 are not consistent with the $\Lambda(1.4) \leq 800$ constraint of GW170817 for the low-spin prior, but are allowed by a more loosely constrained upper limit of 1400 for the high-spin prior (Abbott et al. 2017).

Table 3. NS EOS for the QMF18 model newly introduced in this work.

ϵ [g cm ⁻³]	P [erg cm ⁻³]	ρ_N [fm ⁻³]
0.13855E+15	0.79586E+33	0.082
0.14365E+15	0.85234E+33	0.085
0.15216E+15	0.95144E+33	0.090
0.16920E+15	0.11706E+34	0.100
0.18626E+15	0.14226E+34	0.110
0.20336E+15	0.17145E+34	0.120
0.22047E+15	0.20433E+34	0.130
0.27203E+15	0.33950E+34	0.160
0.32393E+15	0.55426E+34	0.190
0.37631E+15	0.87679E+34	0.220
0.42926E+15	0.13315E+35	0.250
0.48293E+15	0.19385E+35	0.280
0.53741E+15	0.27149E+35	0.310
0.59282E+15	0.36752E+35	0.340
0.64927E+15	0.48329E+35	0.370
0.70686E+15	0.62008E+35	0.400
0.76568E+15	0.77912E+35	0.430
0.82583E+15	0.96151E+35	0.460
0.88738E+15	0.11682E+36	0.490
0.95043E+15	0.13999E+36	0.520
0.10150E+16	0.16569E+36	0.550
0.10813E+16	0.19389E+36	0.580
0.11492E+16	0.22449E+36	0.610
0.12189E+16	0.25733E+36	0.640
0.12904E+16	0.29223E+36	0.670
0.13636E+16	0.32903E+36	0.700
0.14896E+16	0.39423E+36	0.750
0.16207E+16	0.46399E+36	0.800
0.17568E+16	0.53809E+36	0.850
0.18978E+16	0.61645E+36	0.900
0.20438E+16	0.69900E+36	0.950
0.21948E+16	0.78573E+36	1.000
0.25116E+16	0.97160E+36	1.100
0.28480E+16	0.11739E+37	1.200
0.32039E+16	0.13926E+37	1.300

Also, possible strange phase transitions (e.g., Δ -isobars (Zhu et al. 2016)), soften the high-density EOS and lower the maximum static gravitational mass M_{TOV} , leading to relatively small values of $\Lambda(1.4)$: 865 (for DDRHF) vs 828 (for DDRHF Δ).

4. SUMMARY

In the era of gravitational wave astronomy, the unknown EOS of supranuclear matter could soon be understood thanks to accumulating studies on gravity, astrophysics and nuclear physics. The present work timely constructs a new EOS for NSs in the quark level, respecting all available constrains from terrestrial nuclear laboratory experiments and astrophysical observations, including the recent GW170817 constraint on the tidal deformability.

We employ the QMF model, where constituent quarks are confined by a harmonic oscillator confining potential. We first determine the quark potential parameter by reproducing properties of the nucleon in free space. Corrections

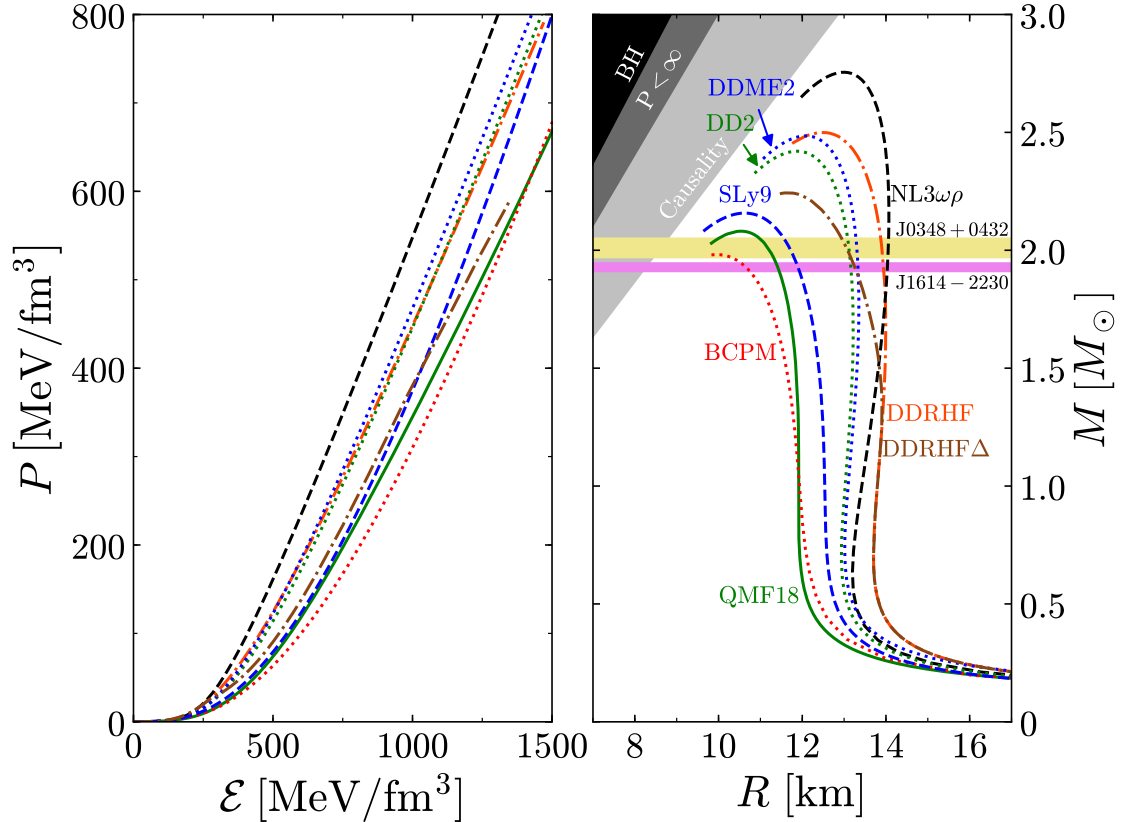


Figure 6. Present new QMF18 EOS (left panel) and its mass-relation (right panel), to be compared with results of other recent NS EOSs from various many-body techniques: DDRHF, DDRHF Δ (Zhu et al. 2016), NL3 $\omega\rho$, DDME2, DD2, Sly9 (Fortin et al. 2016), BCPM (Sharma et al. 2015). The mass measurements for two recent massive stars: PSR J1614-2230 (Demorest et al. 2010; Fonseca et al. 2016) and PSR J0348+0432 (Antoniadis et al. 2013) are also shown. The shaded regions show the black hole limit, the Buchdahl limit and the causality limit, respectively.

Table 4. Radius, compactness and tidal deformability for a $1.4 M_{\odot}$ star are provided for various advanced NS EOSs, together with their maximum static gravitational mass M_{TOV} and the symmetry energy slope L . In the last line we have also shown the range of $\tilde{\Lambda}$ for a binary system with chirp mass equal to $1.188 M_{\odot}$ and mass ratio in the range of $(0.7 - 1)$, which corresponds to the low spin case for GW170817. This calculation shows the consistency between the constraint in $\tilde{\Lambda}$ and $\Lambda(1.4)$. Furthermore, for NL3 $\omega\rho$ EOS which possesses the largest value of $\Lambda(1.4)$ among all the EOSs, $\tilde{\Lambda}$ can actually be as small as 712 if the mass ratio of the system is 0.4 (which corresponds to the 90 % credible range of the mass ratio in the high spin assumption case for GW170817), hence very close to the 90 % credible upper limit for $\tilde{\Lambda}$ in the high spin case. Therefore, the possibility of this EOS wouldn't be clearly excluded if the high spin case is taken into account, as also seen in Nandi & Char (2018).

	QMF18	DDRHF	DDRHF Δ	NL3 $\omega\rho$	DDME2	DD2	Sly9	BCPM
$M_{\text{TOV}} [M_{\odot}]$	2.08	2.50	2.24	2.75	2.48	2.42	2.16	1.98
$L [\text{MeV}]$	40	82.99	82.99	55.5	51.2	55.0	54.9	52.96
$R(1.4) [\text{km}]$	11.77	13.74	13.67	13.75	13.21	13.16	12.46	11.72
$M/R(1.4)$	0.1756	0.1505	0.1512	0.1503	0.1566	0.1571	0.1660	0.1765
$\Lambda(1.4)$	331	865	828	925	681	674	446	294
$\tilde{\Lambda}$	381.4 - 388.4	948.7 - 993.4	900.8 - 962.9	1002.9 - 1056.3	747.8 - 782.7	747.9 - 777.3	519.6 - 524.3	353.9 - 1056.3

due to center-of-mass motion, quark-pion coupling, and one gluon exchange are included to obtain the nucleon mass. Then the many-body nucleonic system is studied in the mean-field level, with the meson coupling constants newly fitted by reproducing the empirical saturation properties of nuclear matter, including the recent determinations of symmetry energy parameters. The predicted star properties can fulfill the recent two-solar-mass constraint and the

800 constraint for the dimensionless tidal deformability of a $1.4 M_{\odot}$ star.

In particular, we explore the relation of the tidal deformability with an uncertain parameter of the symmetry energy slope at saturation. The discussions are done not only for modifying the slope value in its empirical range in one model, but also for comparing results of various many-body techniques. We find no evidence for a simple relation between the symmetry energy slope (hence the radius) and tidal deformability (either $\Lambda(1.4)$ or $\tilde{\Lambda}$). Consequently, claims regarding constraining NS radius with tidal deformability measurements should be considered with caution.

For future perspective, along this line, we can make detailed studies for tidal deformability on the interplay of the saturation parameters with various possible strangeness phase transition at higher densities (usually above $2\rho_0$), e.g., hyperons, kaon condensation, Δ -isobars (Burgio et al. 2011; Hu et al. 2014b; Li et al. 2006, 2007, 2010; Zhu et al. 2016). We can also extend the present study to a unified treatment of both the hadron phase and the quark phase, for exploring better the quark deconfinement phase transition in dense matter and the properties of hybrid star (e.g., Li et al. 2015). An extend QMF18 EOS with unified crust and core properties will be useful as well for supernova simulation or pulsar studies. The pulsar properties can be predicted (e.g., Li et al. 2016a) and updated studies can be done for short gamma-ray bursts (e.g., Li et al. 2016c, 2017). An extension of the current QMF model including a spherical bag for confinement is in progress (Zhu et al. 2018).

We would like to thank Bao-An Li and Antonios Tsokaros for valuable discussions; E. Z. is grateful for China Scholarship Council for supporting the joint Ph.D training project. The work was supported by the National Natural Science Foundation of China (No. U1431107).

REFERENCES

- Abbott, B. P., Abbott, R., Abbott, T. D., et al. 2017, *PhRvL*, 119, 161101
- Ai, S., Gao, H., Dai, Z.-G., et al. 2018, arXiv:1802.00571
- Annala, E., Ecker, C., Hoyos, C., et al. 2018, *PhRvL*, 120, 172703
- Annala, E., Gorda, T., Kurkela, A., & Vuorinen, A. 2017, arXiv:1711.02644
- Antoniadis, J., Freire, P. C. C., Wex, N., et al. 2013, *Sci*, 340, 448
- Baldo, M. 1999, *Nuclear Methods and the Nuclear Equation of State*, 8, 1
- Barik, N., & Dash, B. K. 1986, *PhRvD*, 33, 1925
- Barik, N., Mishra, R. N., Mohanty, D. K., Panda, P. K., & Frederico, T. 2013, *PhRvC*, 88, 015206
- Baym, G., Pethick, C., & Sutherland, P. 1971, *ApJ*, 170, 299
- Bauswein, A., Just, O., Janka, H.-T., & Stergioulas, N. 2017, *ApJL*, 850, L34
- Boguta, J., & Bodmer, A. R. 1977, *NuPhA*, 292, 413
- Burgio, G. F., Schulze, H.-J., & Li, A. 2011, *PhRvC*, 83, 025804
- Centelles, M., Roca-Maza, X., Viñas, X., & Warda, M. 2009, *PhRvL*, 102, 122502
- Chen, L. W., private communication
- Chodos, A., Jaffe, R. L., Johnson, K., Thorn, C. B., & Weisskopf, V. F. 1974, *PhRvD*, 9, 3471
- Cozma, M. D., Leifels, Y., Trautmann, W., Li, Q., & Russotto, P. 2013, *PhRvC*, 88, 044912
- Damour, T., & Nagar, A. 2009, *PhRvD*, 80, 084035
- Damour, T., Soffel, M., & Xu, C. 1992, *PhRvD*, 45, 1017
- Danielewicz, P., Lacey, R., & Lynch, W. G. 2002, *Sci*, 298, 1592
- Danielewicz, P., & Lee, J. 2014, *NuPhA*, 922, 1
- Demorest, P. B., Pennucci, T., Ransom, S. M., Roberts, M. S. E., & Hessels, J. W. T. 2010, *Nature*, 467, 1081
- Drago, A., & Pagliara, G. 2018, *ApJL*, 852, L32
- Fattoyev, F. J., Carvajal, J., Newton, W. G., & Li, B.-A. 2013, *PhRvC*, 87, 015806
- Fattoyev, F. J., Piekarewicz, J., & Horowitz, C. J. 2018, *PhRvL*, 120, 172702
- Fonseca, E., Pennucci, T. T., Ellis, J. A., et al. 2016, *ApJ*, 832, 167
- Fortin, M., Providência, C., Raduta, A. R., et al. 2016, *PhRvC*, 94, 035804
- Frederico, T., Carlson, B. V., Rego, R. A., & Hussein, M. S. 1989, *Journal of Physics G Nuclear Physics*, 15, 297
- Guichon, P. A. M. 1988, *Physics Letters B*, 200, 235
- Hinderer, T. 2008, *ApJ*, 677, 1216-1220; Erratum: *ibid.* 2009, *ApJ*, 697, 964
- Hinderer, T., Lackey, B. D., Lang, R. N., & Read, J. S. 2010, *PhRvD*, 81, 123016
- Horowitz, C. J., & Piekarewicz, J. 2001, *PhRvL*, 86, 5647
- Hu, J. N., Li, A., Shen, H., & Toki, H. 2014, *Progress of Theoretical and Experimental Physics*, 2014, 013D02
- Hu, J. N., Li, A., Toki, H., & Zuo, W. 2014, *PhRvC*, 89, 025802
- Krastev, P. G., & Li, B.-A. 2018, arXiv:1801.04620
- Lattimer, J. M., & Prakash, M. 2004, *Sci*, 304, 536
- Lattimer, J. M., & Prakash, M. 2001, *ApJ*, 550, 426
- Li, A., Burgio, G. F., Lombardo, U., & Zuo, W. 2006, *PhRvC*, 74, 055801
- Li, A., Dong, J. M., Wang, J. B., & Xu, R. X. 2016a, *ApJS*, 223, 16
- Li, A., Zhou, X. R., Burgio, G. F., & Schulze, H.-J. 2010, *PhRvC*, 81, 025806
- Li, A., Zuo, W., & Peng, G. X. 2015, *PhRvC*, 91, 035803
- Li, A., Zhang, N. B., Qi, B., & Burgio, G. F. 2016b, arXiv:1610.08770
- Li, A., Zhang, B., Zhang, N.-B., et al. 2016c, *PhRvD*, 94, 083010
- Li, A., Zhu, Z.-Y., & Zhou, X. 2017, *ApJ*, 844, 41
- Li, A., Zuo, W., Mi, A.-J., & G. B. 2007, *Chinese Physics*, 16, 1934
- Li, B.-A., Chen, L.-W., & Ko, C. M. 2008, *PhR*, 464, 113
- Li, B.-A., & Han, X. 2013, *Physics Letters B*, 727, 276
- Li, B.-A., & Steiner, A. W. 2006, *Physics Letters B*, 642, 436
- Li, D., & Pan, Z. 2016, *Radio Science*, 51, 1060
- Li, J. J., Long, W. H., & Sedrakian, A. 2018a, arXiv:1801.07084
- Li, T., Xiong, S., Zhang, S., et al. 2018b, *Science China Physics, Mechanics, and Astronomy*, 61, 031011
- Long, W. H., Sun, B. Y., Hagino, K., & Sagawa, H. 2012, *PhRvC*, 85, 025806
- Müller, H., & Serot, B. D. 1996, *NuPhA*, 606, 508
- Ma, P.-X., Jiang, J.-L., Wang, H., et al. 2017, arXiv:1711.05565
- Margalit, B., & Metzger, B. D. 2017, *ApJL*, 850, L19
- Mishra, R. N., Sahoo, H. S., Panda, P. K., Barik, N., & Frederico, T. 2016, *PhRvC*, 94, 035805
- Mishra, R. N., Sahoo, H. S., Panda, P. K., Barik, N., & Frederico, T. 2015, *PhRvC*, 92, 045203
- Nandi, R., & Char, P. 2018, *ApJ*, 857, 12
- Negele, J. W., & Vautherin, D. 1973, *NuPhA*, 207, 298
- Özel, F., Psaltis, D., Arzoumanian, Z., Morsink, S., & Bauböck, M. 2016, *ApJ*, 832, 92
- Paschalidis, V., Yagi, K., Alvarez-Castillo, D., Blaschke, D. B., & Sedrakian, A. 2018, *PhRvD*, 97, 084038
- Piekarewicz, J. 2010, *Journal of Physics G Nuclear Physics*, 37, 064038
- Postnikov, S., Prakash, M., & Lattimer, J. M. 2010, *PhRvD*, 82, 024016
- Radice, D., Perego, A., Zappa, F., & Bernuzzi, S. 2018, *ApJL*, 852, L29
- Ray, P. S., Chakrabarty, D., Wilson-Hodge, C. A., et al. 2010, *Proc. SPIE*, 7732, 773248
- Ruiz, M., Shapiro, S. L., & Tsokaros, A. 2018, *PhRvD*, 97, 021501
- Saito, K., Tsushima, K., & Thomas, A. W. 2007, *Progress in Particle and Nuclear Physics*, 58, 1
- Serot B. D. & Walecka, J. D. 1986, *Advances in Nuclear Physics*, 16, 1
- Sharma, B. K., Centelles, M., Viñas, X., Baldo, M., & Burgio, G. F. 2015, *A&A*, 584, A103
- Shen, H., & Toki, H. 2002, *NuPhA*, 707, 469
- Shen, H., & Toki, H. 2000, *PhRvC*, 61, 045205
- Shibata, M., Fujibayashi, S., Hotokezaka, K., et al. 2017, *PhRvD*, 96, 123012
- Shlomo, S., Kolomietz, V. M., & Cold, G. 2006, *European Physical Journal A*, 30, 23
- Sun, B. Y., Long, W. H., Meng, J., & Lombardo, U. 2008, *PhRvC*, 78, 065805
- Toki, H., Meyer, U., Faessler, A., & Brockmann, R. 1998, *PhRvC*, 58, 3749
- Tsang, M. B., Zhang, Y., Danielewicz, P., et al. 2009, *PhRvL*, 102, 122701
- Walecka, J. D. 1974, *Annals of Physics*, 83, 491
- Watts, A., Espinoza, C. M., Xu, R., et al. 2015, *Advancing Astrophysics with the Square Kilometre Array (AASKA14)*, 43
- Watts, A., Yu W., Poutanen J, Zhang S., et al. 2018, *Science China Physics, Mechanics, and Astronomy*, in press
- Xing, X., Hu, J., & Shen, H. 2016, *PhRvC*, 94, 044308
- Zhang, N.-B., Li, B.-A., & Xu, J. 2018, arXiv:1801.06855
- Zhang, Z., & Chen, L.-W. 2015, *PhRvC*, 92, 031301
- Zhou, E., Zhou, X., & Li, A. 2018, *PhRvD*, 97, 083015
- Zhu, Z.-Y., & Li, A. 2018, *PhRvC*, 97, 035805
- Zhu, Z.-Y., Li, A., Hu, J.-N., & Sagawa, H. 2016, *PhRvC*, 94, 045803
- Zhu, Z.-Y., Li, A., Hu, J., & Shen, H. 2018, arXiv:1805.04678